RSC Advances

ROYAL SOCIETY OF CHEMISTRY

www.rsc.org/advances

Cite this: DOI: 10.1039/c0xx00000x

www.rsc.org/xxxxxx

COMMUNICATION

Fabrication and Characterization of PNA-DNA Hybrid Nanostructures†

Bramaramba Gnapareddy[a,b], Jang Ah Kim[a,c], Sreekantha Reddy Dugasani[a,b], Anshula Tandon[a,b], Byeonghoon Kim[a,b], Saima Bashar[a,b], Ji Ah Choi[d], Goon Ho Joe[d], Taesung Kim[a,c], Tai Hwan Ha[e], Sung Ha Park[a,b]*

Received (in XXX, XXX) XthXXXXXXXXX 20XX, Accepted Xth XXXXXXXXX 20XX
DOI: 10.1039/b000000x

Although the distinct property and synthesis methodology of peptide nucleic acid (PNA) molecules have been established by extensive studies, the construction of an artificial nanostructure made from PNA have been examined in only a few reports. Here we study the feasibility of constructing PNA-DNA hybrid nanostructures by conventional free solution annealing and substrate assisted growth methods. For conventional free solution annealing, we introduced a 2-step annealing procedure to mitigate the self-aggregation of PNA in the formation of stable PNA-DNA hybrid structures. Atomic force microscopy images revealed the formation of PNA-DNA hybrid nanostructures smaller than normal DNA and the Raman band intensities of hybrid gradually decreased as a few DNA strands were replaced by PNA possibly due to the fast binding property of PNA and the structural stress between PNA and DNA.

Programmed self-assembly of DNA molecules has emerged as a promising means of nanofabrication of complex, patterned structures for use as templates or scaffolds in imposing desired structures on other materials. Peptide nucleic acid (PNA) is an artificially synthesized structural DNA-analogous to a backbone of repeating neutral N-(2-aminoethyl) glycine units linked by peptide bonds, bearing nucleotide bases and a pseudo-peptide backbone.[1, 2] PNA binds to complementary nucleic acids in both anti-parallel and parallel directions due to its neutral backbone charge[3] and follows Watson-Crick base pairing rules similar to those of DNA.[4] Due to the lack of electrostatic repulsion, PNA can hybridize with another PNA or DNA oligomer with selective binding affinity without positive ions in a buffer.[5] PNA-PNA duplexes have a higher thermal stability than DNA-PNA and DNA-DNA duplexes. The unique properties of PNA, such as superior binding affinity to its complementary bases, high sensitivity to a single base mismatch, high chemical stability under increasing temperature and pH level, and high biological stability to nucleases and proteases, make it as a potential candidate for diverse biological, chemical and material science applications. Although PNA has mainly been used in biological applications, such as diagnostics, biotechnology and pharmaceuticals,[6-11] it may also be used as a connector for self-assembly of DNA-based nanostructures.

Hybrid DNA nanostructures with PNA oligomers have extra benefits associated with greater specificity and tighter binding that result in the accurate detection of target sequences. Considering this, we demonstrate the feasibility of constructing a PNA-DNA hybrid 1-dimensional (1D) 5 helix ribbon (5HR) and 2-dimensional (2D) double crossover (DX) based DNA lattices by using a 2-step conventional free solution (CFS) annealing and a substrate assisted growth (SAG) methods. Previously, the helicity of a PNA-DNA duplex was estimated by incorporating PNA sequences into a DNA tile to examine the formation of 2D arrays using a two-DX tile system.[12] Here, we study the structural stability of PNA-DNA hybrid 1D 5HR and 2D DX lattices and carry out a physical analysis of the lattice coverages of both hybrid nanostructures at their monomer concentrations using the SAG method. Coverage analysis of the lattices on a given substrate may serve as a reference in the fabrication of coverage - controllable PNA-DNA hybrid nanostructures.

In our scheme, two distinct PNA-DNA hybrids, that is 1D 5HR and 2D DX structures, were fabricated using the single stranded tiles (SST)[13] and DX tiles with two adjacent duplexes connected by two crossover junctions,[14] respectively. The crystallization processes of 5HR and the DX lattice differ slightly: for 5HR, individual strands directly formed final structures (SST-based design) at a relatively high temperature whilst for the DX lattice, strands first formed tiles, which then assembled into final lattices (tile-based design) at a relatively low annealing temperature. We incorporated single PNA strand into the unit 5HR or DX tiles, denoted as 5HR(L1P) and DX(1-1P), respectively (Fig. 1b). For the two DX tiles, the corresponding sticky-end pairs within DX-1 and DX-2 were interacted as DNA-DNA and DNA-PNA. As mentioned earlier, we used a single step CFS annealing method for DNA and a 2-step for PNA-DNA hybrid structures, which reduced PNA self-aggregation in buffer solution. Detailed structural sequence maps and nucleotides of the PNA-DNA hybrid structures are shown in electronic supplementary information, Figs. S1-S4 and Tables S1, S2.

Cite this: DOI: 10.1039/c0xx00000x

www.rsc.org/xxxxxx

COMMUNICATION

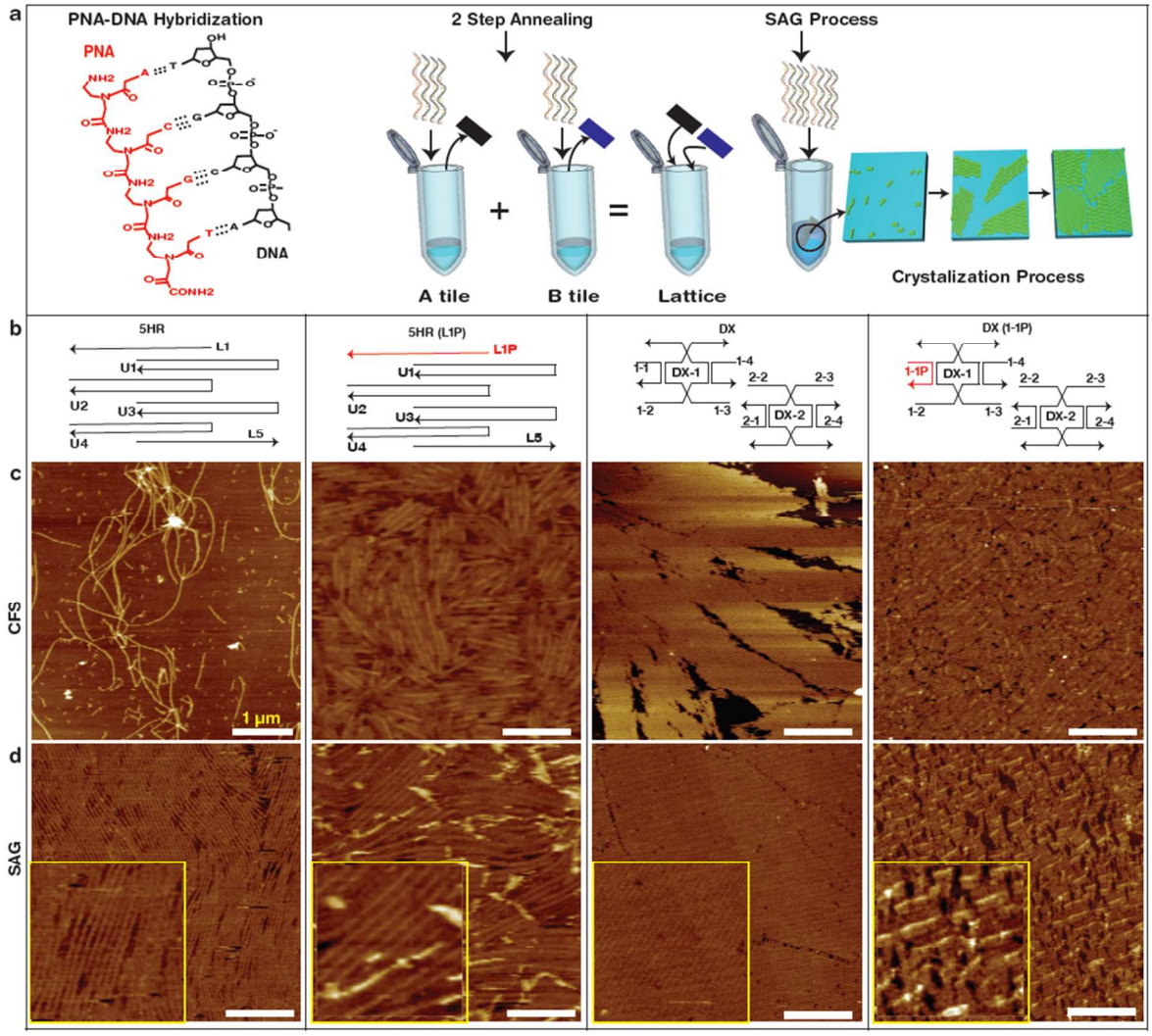

Fig. 1 Schematic diagrams of PNA-DNA duplex, fabrication methodology; unit schematics and AFM images of DNA and PNA-DNA hybrid 5HR and DX nanostructures. (a) A cartoon of PNA-DNA duplex; conventional free solution annealing of 2-step process; substrate assisted growth process. (b-d) Simplified schematics of various DNA and PNA-DNA hybrid 5HR and DX nanostructures with corresponding AFM images. Red and black lines in (b) indicate PNA and DNA strands, respectively. Images in (c) obtained by single step annealing in conventional free solution and (d) by mica assisted growth. Scale bar in the 5HR image in (c) is 1 μm and those in (c) and (d) are 250 nm. Insets in (d) show magnified images with scan sizes of 500 × 500 nm^2.

Additionally we used the recently developed SAG fabrication method[15, 16] for self-assembly to accurately control the coverage of PNA-DNA hybrid as well as normal DNA nanostructures on the mica surface. Both free solution and mica-assisted self-assembly methods were carried out under the similar conditions, except that the latter one was performed at a lower DNA concentration (200 nM for the free solution assembly, and 100 nM for the mica-assisted assembly. 100 nM of either 5HR or DX tiles was enough to cover 5 × 5 mm^2 size of the mica substrate fully). During the annealing process, unit PNA-DNA tiles were laid on the mica substrate randomly and subsequently, the complementary sticky-ends hierarchically assembled with these tiles for structural growth. This led to the formation of large domains of PNA-DNA hybrid structures on the mica substrate possibly by their electrostatic interaction that created a catalytic environment for lattice growth. Fig. 1a represents a schematic illustration of the SAG annealing process and Fig. 1d shows the corresponding AFM images of the polycrystalline domains of the PNA-DNA hybrid 5HR and DX nanostructures on a mica substrate. The surface topologies of the PNA-DNA hybrid structures are clearly distinguishable from normal DNA structures. As shown in inset Fig. 1d, PNA can be clearly observed as bright regions in both the 5HR and DX hybrid nanostructures, which may be due to the absence of a net charge on PNA, which results in a weak binding between the PNA and the charged mica substrate.

In the design and assembly of constructs including PNA strands, we need to take into account the interaction between PNA and

DNA molecules and the structural differences between them, that is, the geometry of the hybrid duplex. The PNA backbone is not charged; hence, these polymers form a stronger bond between PNA–DNA strands than between DNA–DNA strands. This is because of the lack of charge repulsion between PNA and DNA strands. PNA can bind strongly and selectively to complementary DNA in an exclusive antiparallel orientation following the Watson–Crick base pairing rules to target the complementary nucleic acids.[3] Preference for antiparallel orientation is a general feature of a mixed sequence PNA-DNA complex. The neutral PNA molecules also have a tendency to aggregate to a degree depending on the sequence of the oligomer. The PNA–PNA duplex is similar to the antiparallel PNA–DNA duplex and is between that of A- and B-helix. High thermal stability is expected in PNA-DNA hybrid structures, because of the absence of inter-strand repulsions, dipolar interactions, and intra-backbone hydrogen bonds. At the same time, it would be difficult to form large-size lattice of PNA-DNA hybrids because of the geometrical base stacking variations between PNA and DNA molecules. In addition, PNA has a unique helix form, the P-form observed in the PNA–PNA duplex. This helix is wide (0.28 nm) and has a large pitch of 18 base pairs, as observed by X-ray crystallography,[17] in contrast to the pitch of the PNA-DNA duplex of 13 base pairs, as observed by NMR.[18] Thus, PNA-DNA hybridization results in a structural curvature stress that restricts the formation of larger size lattices.

We also checked the feasibility of fabricating PNA-DNA hybrids by incorporating more than one PNA strand into DX lattices shown in Fig. 2. Thus DX whose strands 1-1 and 2-1 were replaced by PNA strands was represented as DX(1-1P, 2-1P); DX whose strands 1-1 and 2-4 were replaced by PNA was represented as DX(1-1P, 2-4P) and DX with four strands replaced by PNA was represented as DX(1-1P, 1-4P, 2-1P, 2-4P). Corresponding sticky-end pair interactions for DX(1-1P, 2-1P) were DNA-PNA and DNA-PNA; for DX(1-1P, 2-4P), DNA-DNA and PNA-PNA; and for DX(1-1P, 1-4P, 2-1P, 2-4P), PNA-PNA and PNA-PNA.

If DX(1-1P, 2-1P) or DX(1-1P, 2-4P) hybrid lattices were annealed by the single-step CFS annealing method, structures did not form properly. Two PNA strands in a test tube restrict the formation of periodic DNA-PNA structures but promote the formation of aggregates. So we fabricated them by the 2-step CFS annealing method; the schematics of the DX tiles and the corresponding AFM images for the 2-step CFS annealing are shown in Fig. 2a and 2b (first two columns). For the 2-step, the first step involved high-temperature annealing of equimolar mixtures of strands of DX-1 and DX-2 tiles of 400 nM tile concentration, each in two different test tubes. They were cooled slowly from 95°C to 25°C by placing test tubes in a Styrofoam box containing 2 L of boiled water for at least 24 hours to facilitate hybridization. The second step involved low-temperature annealing, with the same volume of DX-1 and DX-2 tiles. Now each tile concentration became 200 nM; they were cooled slowly from 40°C to 25°C by placing a tube in a Styrofoam box containing 2 L of boiled water (initial temperature, 40°C) for 24 hours to assemble PNA-DNA hybrid nanostructures. The second step of the annealing process prevented PNA aggregation. When DX(1-1P, 2-1P) or DX(1-1P, 2-4P) hybrid nanostructures were fabricated on a mica substrate by the SAG method, we observed the PNA-DNA hybrid lattices as shown in Fig. 2c. Even two PNA strands replaced in DX structures, there is a possibility for formation of hybrid structures using the SAG method. This might be due to the electrostatic interaction between the mica and hybrid lattices which was strong enough to protect from PNA self-aggregation. Information regarding experimental details, the structural sequence map and nucleotides of PNA-DNA hybrid structures is given in the electronic supplementary information, Figs. S5-S7, and Tables S1, S2.

Next, we tried to fabricate DX(1-1P, 1-4P, 2-1P, 2-4P) hybrid structures (each DX tile contains two PNA strands) by the CFS and the SAG annealing methods; the schematics and corresponding AFM images are shown in Fig. 2a-c (last column). As expected, self-assembly failed and random aggregates were obtained. These amorphous and aggregated structures were clearly evident from the AFM images in Fig. 2b and 2c. These aggregates could have been formed due to the intrinsic physicochemical property of PNA, which usually forms random aggregates at higher temperatures. Thus when more than two DX strands were replaced by PNA, locally, small fragments (amorphous nature) of the lattice structures were observed, which could have been due to the higher structural curvature stress by the different numbers of base pairs per one full turn in PNA-PNA, PNA-DNA and DNA-DNA hybridizations.

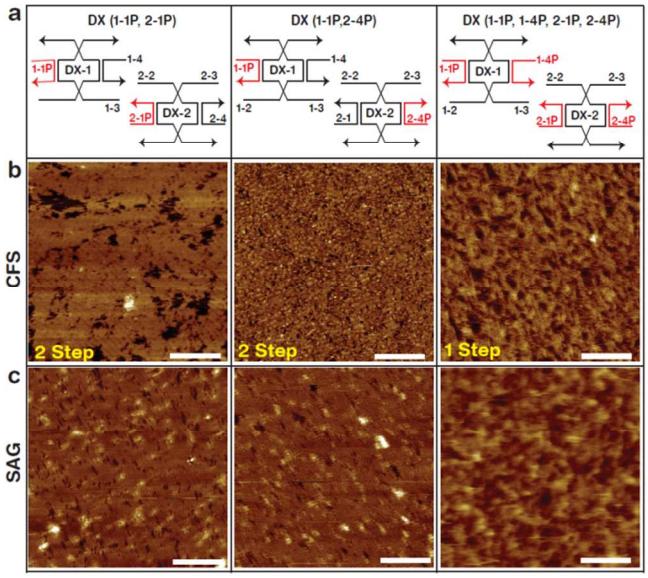

Fig. 2 Schematic diagrams of unit PNA-DNA tiles, and AFM images of 2 and 4 PNA strands in the DX hybrid structures. (a) Simplified schematics of three different configurations of PNA-DNA hybrid DX nanostructures with corresponding AFM images. Red and black lines in (a) indicate PNA and DNA strands, respectively. Images in (b) obtained by single- or double- step annealing in conventional free solution and (c) by mica assisted growth. All scale bars in images are 250 nm.

The coverage dependence on the DX monomer concentration for the SAG method was studied to better understand the lattice growth mechanism. Hence, the lattice coverage for the hybrid 5HR(L1P), DX(1-1P), DX(1-1P, 2-1P), and DX(1-1P, 2-4P) nanostructures was analyzed for various monomer concentrations. Although DX(1-1P, 2-1P) and DX(1-1P, 2-4P) contain a PNA strand in each DX tile, single step (one-pot) annealing with the SAG can make the DX lattices safely due to the catalytic effect by the substrate. Monomer concentration is directly related to the lattice coverage of a hybrid nanostructure. To achieve consistency and reliability, four reference conditions were fixed during the process: substrate size (5 mm × 5 mm), total PNA-DNA sample volume (250 μL), temperature gradient and time (95°C to 25°C for 24 h). On the other hand, the monomer concentration, which was used as the control parameter, was varied. The hybrid structures started to assemble at the monomer threshold concentrations C_{th} of 2 nM for DX(1-1P) and DX(1-1P, 2-1P) and 5 nM for 5HR(L1P) and DX(1-1P, 2-4P). Consequently, full

lattice coverage was achieved at monomer saturation concentrations C_s of 20 nM for 5HR(L1P) and DX(1-1P, 2-4P) and about 30 nM for DX(1-1P), and DX(1-1P, 2-1P) as shown in Fig. 3. In the SAG system, DNA molecules start to nucleate on the substrate at around 2-5 nM (C_{th}), whereas in CFS, at around 40 nM. This was due to the catalytic behavior of the substrate, which pays a partial entropic cost for hybrid crystallization via the Coulomb force between the charged substrate and the charged 5HR strands or DX tiles. This force creates relatively a higher PNA-DNA molecular density close to the substrate than in the rest of the solution, thus providing the proper environment for crystallization.

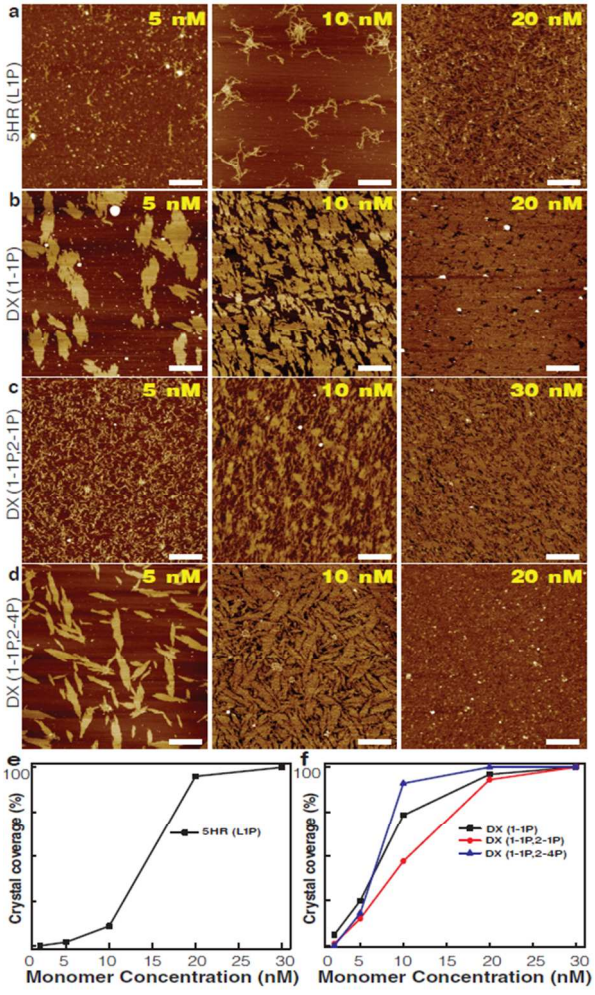

Fig.3 AFM images and lattice coverage on mica substrate. (a-d) AFM images of PNA-DNA hybrid 5HR and DX nanostructures grown at various monomer concentrations by mica assisted growth method. All scale bars in images are 500 nm. (e, f) Lattice coverage of PNA-DNA hybrid 5HR and DX nanostructures at various monomer concentrations.

In order to comprehend the binding mechanism between PNA and DNA molecules, we performed Raman spectroscopy. Raman band positions of mica and DNA on mica were observed to be pretty similar to each other (electronic supplementary information, Fig. S8), as mica consists of minerals and other metallic impurities. Thus to overcome the undesirable substrate effects of mica, a glass substrate was introduced for reliable Raman analysis. In this experiment, the spectrum was excited by a green laser at 532 nm, and was measured by the intensities of the bands in the wave number range between 400 and 2000 cm^{-1}. This wave number range of the Raman spectrum consists of almost all the fundamental vibrational bands of DNA molecules. The Raman spectra of 5HR and DX hybrid nanostructures are shown in Fig. 4a and 4b. The pristine 5HR showed the vibration and stretching Raman bands centered around 1246, 1381 and 1420 cm^{-1} for adenine (*A*); 742, 770, 1291 and 1469 cm^{-1} for thymine (*T*); 930, 1381 and 1585 cm^{-1} guanine (*G*); 1291, 1348 and 1617 cm^{-1} for cytosine (*C*); and 1066 cm^{-1} for the phosphate backbone (PO_4^-). The pristine DX nanostructure showed the vibration and stretching Raman bands centered around 1246 and 1420 cm^{-1} for *A*; 420, 770, and 1469 cm^{-1} for *T*; 655, 930, and 1585 cm^{-1} for *G*; 619 and 1348 cm^{-1} for *C*; and 1066, and 1145 cm^{-1} for PO_4^-.[19,20,21]

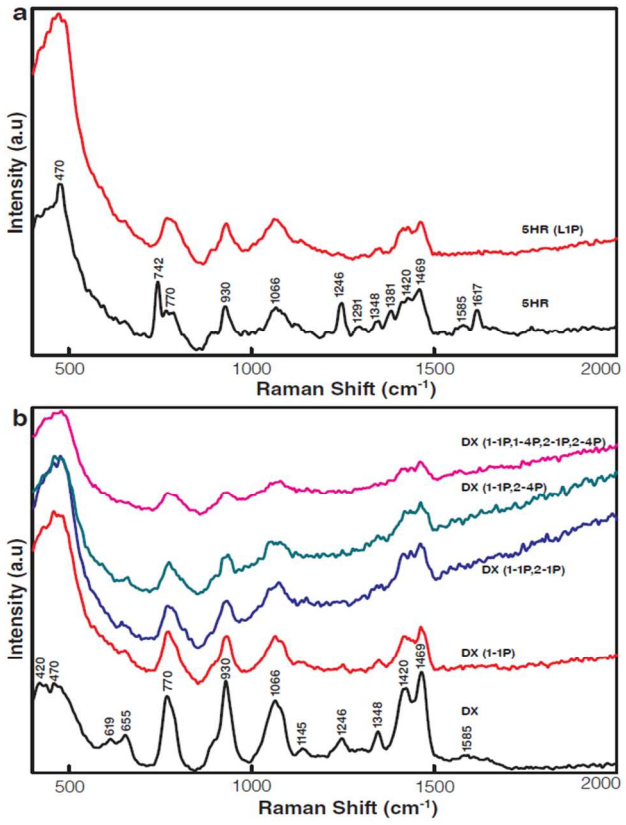

Fig. 4 The Raman spectra of glass assisted grown PNA-DNA hybrid 5HR and DX nanostructures. (a) The graph represents the Raman spectra of 5HR and 5HR(L1P) PNA-DNA hybrid ribbons. (b) The Raman spectra of DX, DX(1-1P), DX(1-1P, 2-1P), DX(1-1P, 2-4P) and DX(1-1P, 1-4P, 2-1P, 2-4P) PNA-DNA hybrid lattices.

Raman spectra of PNA-DNA hybrid nanostructures were generated to trace the variations in the intensity of the Raman bands upon interaction of DNA and PNA molecules. There was a considerable decrease in the intensity of the Raman bands throughout the spectra when relatively large numbers of PNA strands were incorporated into the PNA-DNA hybrid nanostructures. This decrease was due to the incorporated PNA, which dramatically changed the lattice periodicity. This change in lattice periodicity deformed the lattice structure and made the lattice amorphous. Another crucial factor that differentiates DNA and PNA-DNA hybrid structures is their backbones. We assumed initially that the changes in the intensity might have been only due to the backbone bands, but surprisingly, the results of Raman data showed that it occurred in all the bands as more PNA strands were added. When two DX strands were replaced by PNA in a PNA-DNA hybrid structure, *i.e.*, DX(1-1P, 1-4P, 2-1P, 2-4P), the Raman band intensities showed a significant decrease, which was due to the reduced yield of the hybrid structure. Interestingly, we

could not find any secondary phases of PNA bands in all the Raman spectra. This implies that both PNA and DNA molecules act as a single system to promote the formation of PNA-DNA hybrid 5HR and DX nanostructures. The significant decrease in Raman band intensities due to the incorporation of more PNA molecules resulted in structural curvature stress, and this stress was the reason for the structural deformation of the hybrid nanostructure or its amorphous nature, which was clearly evident in the AFM images.

In conclusion, we demonstrated the construction of PNA-DNA hybrid 5HR and DX nanostructures by using CFS and SAG methods. The AFM results revealed the topological formation of 1D ribbons and 2D lattices, and the Raman band intensities showed the tendency for PNA-DNA hybridization. The hybrid structures were successfully fabricated when one strand in unit building block was replaced by PNA, but upon addition of more than one PNA strands into the DX tile, hybrid structures did not form properly, but instead small amorphous fragments were formed in the lattice structures (CFS). This can be explained by the increased structural curvature stress due to distinct base pairs in the duplex, self-aggregation of PNA during the annealing process, and by the various thermal stabilities and melting temperatures between the hybrid nanostructures. These PNA-DNA hybrid nanostructures may be used in applications where traditional synthetic DNA and PNA have been used, with PNA providing additional benefits, such as tighter binding, greater specificity, stability and accurate detection of target sequences. At the same time, our design strategy may aid in the use of the rich functional possibilities of unnatural oligomeric variants of DNA molecules in structural nucleic acid nanotechnology.

Acknowledgement

This paper was supported by Faculty Research Fund, Sungkyunkwan University, 2011.

Notes and references

[a] Sungkyunkwan Advanced Institute of Nanotechnology (SAINT), Sungkyunkwan University, Suwon 440-746, Korea
[b] Department of Physics, Sungkyunkwan University, Suwon 440-746, Korea. E-mail: sunghapark@skku.edu
[c] School of Mechanical Engineering, Sungkyunkwan University, Suwon 440-746, Korea
[d] Panagene Inc., Daejeon 305-510, Korea
[e] Research Center of Integrative Cellulomics, Korea Research Institute of Bioscience and Biotechnology (KRIBB), Daejeon 305-806, Korea

†Electronic Supplementary Information (ESI) available: Sample preparation; schematic diagram for DX; sequences pool and sticky-ends of DX tiles used in this experiment; the Raman spectra of glass, mica and DNA on mica; See DOI: 10.1039/b000000x/.

1. P. E. Nielsen, M. Egholm, R. H. Berg, and O. Buchardt, *Science* 1991, **254**, 1497.
2. M. Egholm, O. Buchardt, L. Christensen, C. Behrens, S. M. Freier, D. A. Driver, R. H. Berg, S. K. Kim, B. Norden, and P. E. Nielsen, *Nature* 1993, **365**, 566.
3. V. Tirayut, and S. Choladda, *Org. Lett.* 2006, **8**, 1897.
4. P. E. Nielsen, and M. Egholm. *Current Issues Molec. Biol*. 1999, **1**, 89.
5. K. K. Jensen, H. Orum, P. E. Nielsen, and B. Norden, *Biochemistry* 1997, **36**, 5072.
6. E. Rockenbauer, K. Petersen, U. Vogel, L. Bolund, S. Kolvraa, K. V. Nielsen, and N. B. Anderson, *Cytometry* 2005, **64A,** 80.
7. Z. C. Liu, D. S. Shin, M. Shokouhimehr, K. N. Lee, B. W. Yoo, Y. K. Kim, and Y. S. Lee, *Biosensors and Bioelectronics* 2007, **22**, 2891.
8. F. R. Raymond, H. A. Ho, R. Peytavi, L. Bissonnette, M. Boissinot, F. J. Picard, M. Leclerc, and M. G. Bergeron, *BMC Biotechnol*. 2005, **5**, 10.
9. J. Kurreck, *Eur. J. Biochem*. 2003, **270**, 1628.
10. A. T. Salazar, J. Dhawan, A. Lovejoy, Q. A. Liu, and A. N. Gifford, *Anal. Biochem.* 2007, **360**, 92.
11. H. Kuhn, Y. Hu, M. D. F. Kamenetskii, and V. V. Demidov, *Biochemistry* 2003, **42**, 4985.
12. P. S. Lukeman, A. C. Mittaland, N. C. Seeman, *Chem. Comm.* 2004, 1694.
13. P. Yin, R. F. Hariadi, S. Sahu, H. M. Choi, S. H. Park, T. H. LaBean, and J. H. Reif, *Science* 2008, **321**, 824.
14. E. Winfree, F. Liu, L. A. Wenzler, and N. C. Seeman, *Nature* 1998, **394**, 539.
15. S. R. Dugasani, N. H. Lee, J. Lee, B. H. Kim, S. U. Hwang, K. W. Lee, W. N. Kang, and S. H. Park, *Sci. Rep*. 2013, **3**, 1819.
16. J. Lee, S. Kim, J. Kim, C.-W. Lee, Y. Roh, and S. H. Park, *Angew. Chem. Int. Ed.* 2011, **50**, 9145.
17. H. Rasmussen, J. S. Kastrup, J. N. Nielsen, J. M. Nielsen, and P. E. Nielsen, *Nat. Struct. Biol*. 1997, **4**, 98.
18. M. Eriksson, and P. E. Nielsen, *Nat. Struct. Biol*. 1996, **3**, 410.
19. C. Otto, T. J. J. Van den Tweel, F. F. M. De Mul, and J. Greve, *J. Raman Spectrosc.* 1986, **17**, 289.
20. M. Vasudev, T. C. Wu, S. Biswas, D.Mitra, M. A. Stroscio, S. Guthrie, M. Reed, K. P. Burris, and C. N. Stewart, *IEEE Trans. Nanotechnol.* 2011, **10**, 35.
21. S. R. Dugasani, J. A. Kim, B. H. Kim, P. J. Rao, B. Gnapareddy, C. Vyas, T. S. Kim, S. H. Park, and V. Manchanda, *ACS Appl. Mater. Interfaces* 2014, **6**, 2974.

Table of Contents Graphic

The feasibility of constructing PNA-DNA hybrid nanostructures by conventional free solution annealing and substrate assisted growth methods was studied.